

Establishing process-structure linkages using Generative Adversarial Networks

Mohammad Safiuddin^a, CH Likith Reddy^b, Ganesh Vasantada^c, CHJNS
Harsha^d, Srinu Gangolu^{e,*}

^a*National Institute of Technology Calicut*

^b*National Institute of Technology Calicut*

^c*National Institute of Technology Calicut*

^d*National Institute of Technology Calicut*

^e*National Institute of Technology Calicut*

Abstract

The microstructure of material strongly influences its mechanical properties and the microstructure itself is influenced by the processing conditions. Thus, establishing a Process-Structure-Property relationship is a crucial task in material design and is of interest in many engineering applications. We develop a GAN (Generative Adversarial Network) to synthesize microstructures based on given processing conditions. This approach is devoid of feature engineering, needs little domain awareness, and can be applied to a wide variety of material systems. Results show that our GAN model can produce high-fidelity multi-phase microstructures which have a good correlation with the given processing conditions.

Keywords: Generative Adversarial Network, Conditional Image synthesis, processing-structure relationship, Deep learning, microstructure

1. Introduction

A significant emphasis in the design of advanced material systems is the delineation of process-structure-property relationships [1]. Although analytical

*Corresponding author. Tel.: +91 495 2286437

URL: srinu@nitc.ac.in (Srinu Gangolu)

and statistical methods for the design of some materials have been success-
fully used [2], the underlying assumptions of homogeneity restrict their ability
5 to generalize to other material systems. As solutions to these challenges, ma-
chine learning and data-driven approaches have piqued interest in the field of
material science. Microstructure reconstruction is important in computational
material design because it provides an effective method for understanding the
10 high-dimensional microstructure space. Deep learning has been used in the
past to model material properties from microstructures [3] and to synthesise
microstructures with desirable properties [4, 5].

Deep learning-based microstructure reconstruction relies heavily on genera-
tive models like variational autoencoders (VAE) [6] and generative adversarial
15 networks (GAN) [7]. VAE was used by Cang et al. [4] to create two-phase
microstructures, demonstrating the ability of convolutional networks to model
material characteristics from microstructures. To synthesise microstructures,
Yang et al. [5] used deep convolutional GAN and transfer learning to enhance
structure-property predictions.

20 The aforementioned line of work does not account for two aspects of the
problem at hand. Previous research has concentrated on two-phase microstruc-
tures, while multiphase microstructures are present in many material systems.
Characterization and generation of multiphase microstructures have been stud-
ied rarely, owing to the difficulty of determining the higher order correlation
25 of multiphase materials. Also, recent research has not considered the impact
of processing conditions on the microstructure. This is a critical component of
material design since the interest is to not only design an ideal microstructure
but also to figure out how to produce it.

We overcome these two problems by creating a GAN architecture capable
30 of synthesising multiphase alloy microstructures from processing conditions and
illustrate this approach by using the Ultra High Carbon Steel Database [8].
This is the first attempt, to our knowledge, to represent the processing-structure
relationship as a multi-conditional image synthesis problem.

2. Methodology

35 2.1. The Ultra High Carbon Steel Database (UHCSDB)

The UHCS database contains 961 microstructures produced by scanning electron microscopy (SEM) of samples with similar compositions but different processing conditions. These steels have a carbon content of 1-2.1% per cent, and the steel grade used in this dataset is Adamite grade steel (AS100). Due
40 to the increased carbon concentration of these alloys in comparison to standard steels, pro eutectoid cementite (Fe_3C) produces a carbide network coupled with the grain boundaries of the high-temperature austenite process and is a distinguishing microstructure feature of these alloys. These brittle, powerful carbides contribute to the well-known strength and wear resistance of ultra-high carbon
45 steel [9]. Various microconstituents found in the dataset are shown in figure 1.

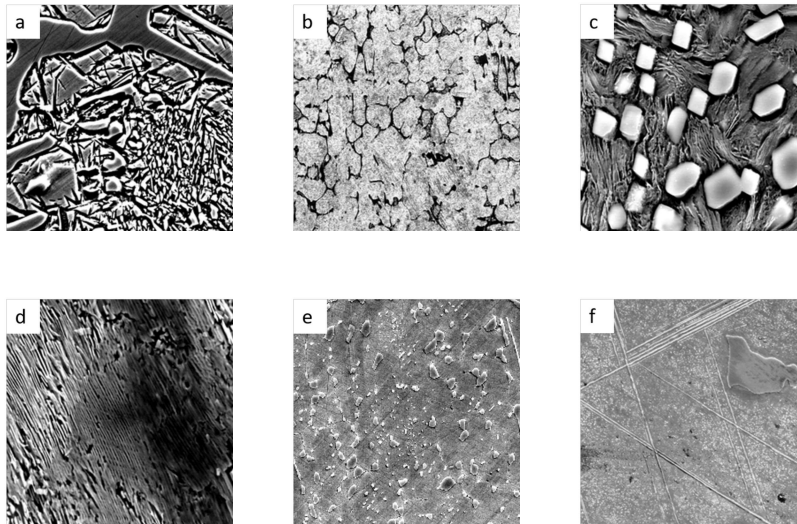


Figure 1: Primary microstructure constituents in the UHCS dataset: a) Pearlite, b) Cementite Network, c) Spheroidite, d) Pearlite + Spheroidite, e) Widmanstätten, f) Martensite

Out of the 961 images present, 598 images have metadata on processing conditions in the form of three parameters *i.e.* annealing temperature, anneal-

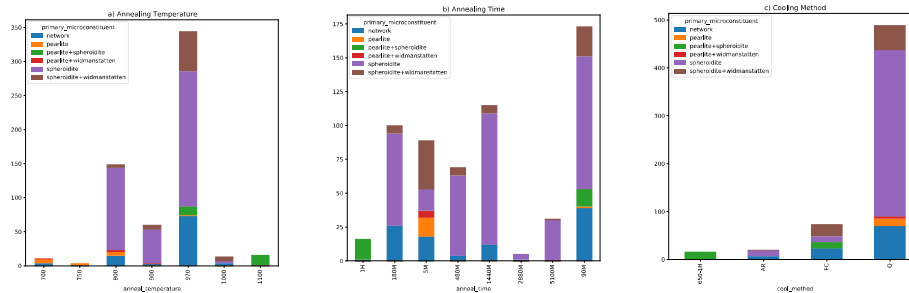


Figure 2: Stacked bar plots for process parameters. Imbalance in the dataset can be clearly seen.

ing time and the cooling method. It is evident from figure 2 that spheroidite
 50 is the major micro constituent in many classes. This imbalance poses an issue to the GAN which can be solved by eliminating samples from the majority class (under-sampling) or adding more examples from the minority class (over-sampling). Over-sampling can cause overfitting while under-sampling can cause a loss in information. Therefore, when sampling from an unbalanced dataset,
 55 we rebalance the class distributions and mitigate overfitting using data augmentations. Owing to the small size of the dataset, using a deep learning model like GAN effectively, is a challenging task. We can overcome this to an extent using DiffAugment [10] with Colour, Translation and Cutout policy.

60 2.2. Learning Framework

To learn underlying latent distributions from high dimensional data, such as images, GANs formulate the learning problem as a two-player zero-sum game between a generator which tries to produce synthetic images indistinguishable from real ones and a discriminator which tries to differentiate if an image is real
 65 or has been synthesised. Conditional generative models also offer an effective way to better manage features in synthesised samples by imposing additional structure onto the GAN latent space. Conditional GAN [11] suggests an adaptation of this technique by supplying side details (class labels) to both the generator and discriminator. This increases the consistency and variety of the

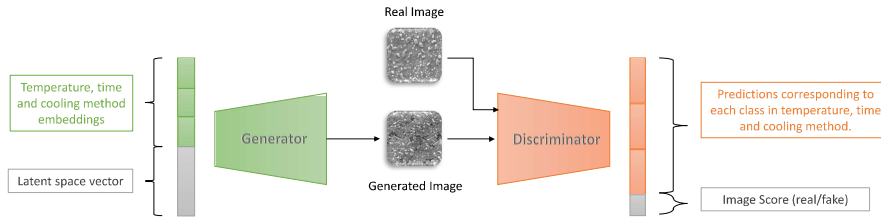


Figure 3: Overview of the GAN framework used to synthesize microstructures based on processing conditions.

70 synthesised images. Following Goodfellow et al’s [7] introduction of GAN, several improvements have been proposed in order to promote consistent training and rapid convergence. An overview of the GAN framework is shown in figure 3.

Architecture. BigGAN [12] improves efficiency by introducing general architectural improvements for better scalability and by modifying a regularisation scheme to improve conditioning. This current work builds on the BigGAN-
75 deep architecture to create microstructures from specified processing parameter values. The generator’s input mechanism was modified to accommodate three conditional inputs as opposed to just one. The discriminator was modified to
80 output a 21-dimensional vector (refer to Loss function) as output instead of a scalar. The aforementioned modifications are described in more detail in Appendix A.

Loss function. We use Omni loss [13] instead of hinge-loss used in the BigGAN paper [12]. Loss function can be elucidated as follows.

Let \hat{y} and y denote a classifier output and the corresponding multi-label vector respectively. . Assume you have K positive labels and L negative labels. Then \hat{y} is a score vector with $K + L$ dimensions.. The omni-loss is defined as

$$\mathcal{L}_{\text{omni}}(\hat{\mathbf{y}}, \mathbf{y}) = \log \left(1 + \sum_{i \in I_{\text{neg}}} e^{\hat{y}_i} \right) + \log \left(1 + \sum_{j \in I_{\text{pos}}} e^{-\hat{y}_j} \right) \quad (1)$$

85 I_{neg} contains indexes of negative scores (i.e., $|I_{\text{neg}}| = L$), and I_{pos} contains indexes of positive scores (i.e., $|I_{\text{pos}}| = K$). \hat{y}_k represents the element k of vector \hat{y} . Using Eq. 1 we can define the loss for both the generator and discriminator.

The discriminator loss is composed of two parts, one for x_{real} (from training set) and another for x_{fake} (from generator). The multi-label vector associated with x_{real} is given by

$$\mathbf{y}_{\text{real}} = \underbrace{[-1, \dots, 1_{\text{gt}_{\text{temp}}}, \dots, -1]}_{C_{\text{temp}}}, \underbrace{[-1, \dots, 1_{\text{gt}_{\text{time}}}, \dots, -1]}_{C_{\text{time}}}, \underbrace{[-1, \dots, 1_{\text{gt}_{\text{cool}}}, \dots, -1]}_{C_{\text{cool}}}, \underbrace{[1_{\text{real}}, -1]}_2 \quad (2)$$

$C_{\text{temp}}, C_{\text{time}}, C_{\text{cool}}$ are the number of classes in anneal temperature, anneal time and cooling method respectively. The dimension of \mathbf{y}_{real} is given by $C = C_{\text{temp}} + C_{\text{time}} + C_{\text{cool}} + 2 = 7 + 8 + 4 + 2 = 21$. The value of $1_{\text{gt}_{\text{temp}}}, 1_{\text{gt}_{\text{time}}}$ and $1_{\text{gt}_{\text{cool}}}$ is 1 if index in the vector is equal to the ground truth label of x_{real} , else -1 . 1 is used to denote that the corresponding score belongs to the positive set and -1 is used for the negative set. The multi-label vector for x_{fake} is also a 21 dimensional vector and is given by

$$\mathbf{y}_{\text{fake}} = \underbrace{[-1, \dots, -1, \dots, -1]}_{C_{\text{temp}}}, \underbrace{[-1, \dots, -1, \dots, -1]}_{C_{\text{time}}}, \underbrace{[-1, \dots, -1, \dots, -1]}_{C_{\text{cool}}}, \underbrace{[-1, 1_{\text{fake}}]}_2 \quad (3)$$

From Eq. 1, 2, 3, we can define discriminator loss as follows

$$\mathcal{L}_D = E_{\mathbf{x}_{\text{real}} \sim p_d} [\mathcal{L}_{\text{omni}} (D(\mathbf{x}_{\text{real}}), \mathbf{y}_{\text{real}})] + E_{\mathbf{x}_{\text{fake}} \sim p_g} [\mathcal{L}_{\text{omni}} (D(\mathbf{x}_{\text{fake}}), \mathbf{y}_{\text{fake}})] \quad (4)$$

The generator intends to deceive the discriminator into thinking the samples are real. As a result, the multi-label vector is

$$\mathbf{y}_{\text{fake}}^{(G)} = \underbrace{[-1, \dots, 1_{\text{G}_{\text{temp}}}, \dots, -1]}_{C_{\text{temp}}}, \underbrace{[-1, \dots, 1_{\text{G}_{\text{time}}}, \dots, -1]}_{C_{\text{time}}}, \underbrace{[-1, \dots, 1_{\text{G}_{\text{cool}}}, \dots, -1]}_{C_{\text{cool}}}, \underbrace{[1_{\text{real}}, -1]}_2 \quad (5)$$

90 The value of $1_{\text{G}_{\text{temp}}}, 1_{\text{G}_{\text{time}}}$ and $1_{\text{G}_{\text{cool}}}$ is 1 if index in the vector is equal to the label used by the generator to generate x_{fake} , else -1 . The generator loss

is given by

$$\mathcal{L}_G = E_{\mathbf{x}_{\text{fake}} \sim p_g} \left[\mathcal{L}_{\text{omni}} \left(D(\mathbf{x}_{\text{fake}}), \mathbf{y}_{\text{fake}}^{(G)} \right) \right] \quad (6)$$

Training. We use Adam optimizer [14] with a learning rate of 0.0002, $\beta_1 = 0.9$ and $\beta_2 = 0.999$ for both the generator and discriminator. Additionally, the weight decay of the generator and discriminator is set to 0.001 and 0.0005, respectively. Model is trained for 6000 epochs with a batch size of 96 and a $D : G$ ratio of 4 : 1. The implementation was done using Pytorch [15] and it was trained on the free GPU available on Kaggle ¹.

3. Results

After adequate training, the GAN model’s generator component generates microstructures that visually mimic the intricacy of the original microstructures with surprising realism. While the GAN-generated microstructures and the original data appear to be extremely comparable, a closer examination reveals that the original microstructures are more variable than the synthetic microstructures. This is consistent with observations demonstrating that GANs produce less variance than the data used to train them [16]; they learn the average structure more quickly than the outliers. Nonetheless, the created microstructures resemble those in the training set. Also, It is evident from figure 4 that there a strong correlation between the processing parameters and the generated microstructures. The characteristics of the generated microstructures that are worth noting are described in Discussion .

Notation for processing conditions. Let us consider: 800-5-Q, where the anneal temperature is 800°C, anneal time is 5 minutes and cooling method is Quenching. Cooling methods present in the dataset are Quenching, Air Cooling, Furnace Cooling and constant heating at 650°C for 1 hour which are represented as Q, AR, FC, 650-1H respectively.

¹www.kaggle.com

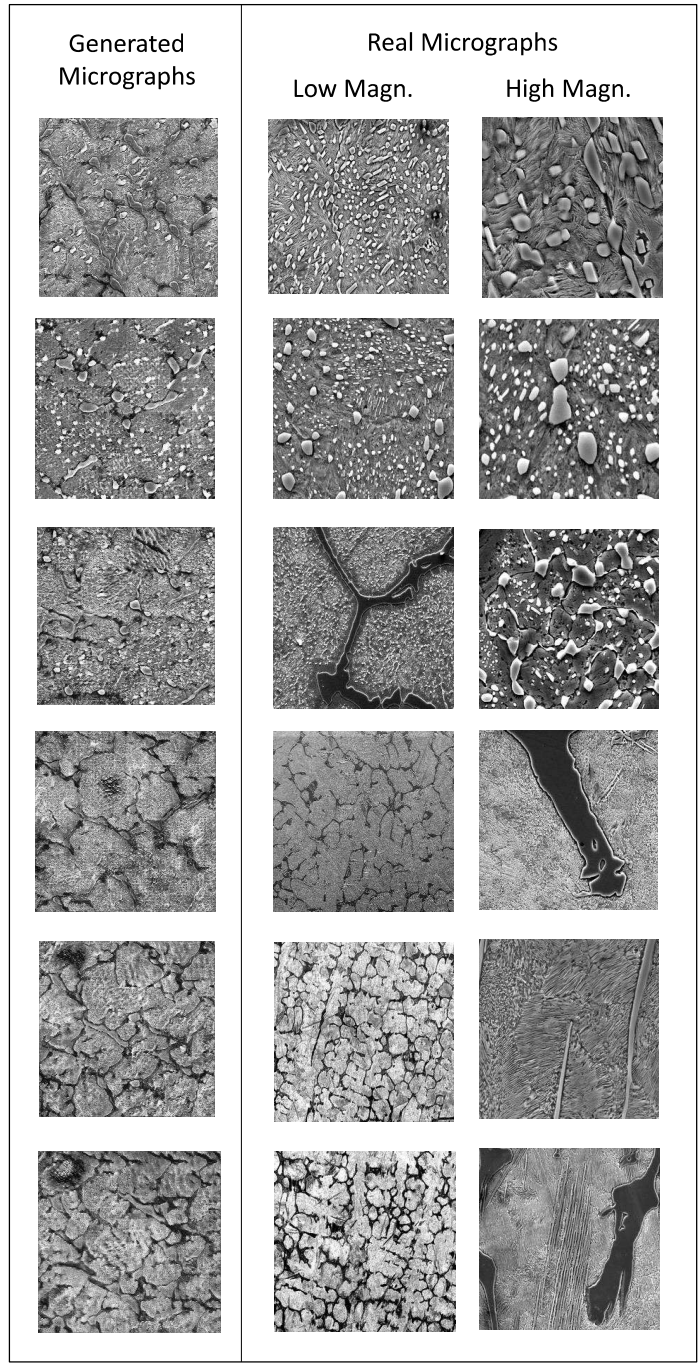


Figure 4: A visual comparison of generated microstructures with the real ones in the dataset.

4. Discussion

Effect of Magnification. The training data consists of images with varying magnifications. The current GAN model adapts to this in a peculiar manner. The relative scale of a certain feature with respect to other feature in a generated microstructure is similar to the microstructures in the dataset. Let us consider the case represented in figure 5. Spheroidite grains can be clearly seen in figure 5c. However, there is a network structure in figure 5b and the spheroidite is not clearly visible. The generated image has a level of magnification where both spheroidite and network can be seen. The size of spheroidite grains is much smaller compared to the ones in figure 5c and the network web is less spread out compared to figure 5b. This adaptability is seen across other processing parameters as well (see figure 4).

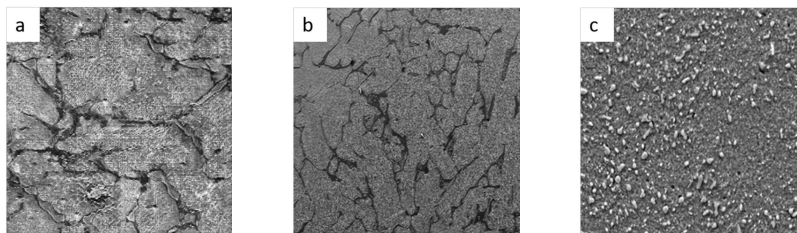


Figure 5: Microstructures corresponding to 800-1440-Q: a) Generated, b) Real (Magn. 98x), c) Real (Magn. 1964x).

Microstructure Evolution. To understand if the model has learnt any physically accurate patterns based on the changes in the processing conditions, let us consider the case in figure 6. It can be observed that, as the annealing time increases, the size of the sphere keeps on increasing by combining with nearby spheres. This phenomenon is in line with the work of Hecht et al.[17] though not completely consistent from 60M to 90M.

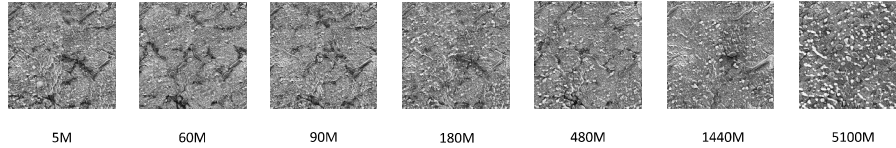


Figure 6: Generated microstructures corresponding to 1000- X -Q, where X is increased from 5 minutes to 5100 minutes.

135 5. Conclusion

We used a modified version of the BigGAN-deep architecture with a re-framed Omni loss to generate microstructures under specific conditions. We demonstrate the fidelity of the generated microstructures and their correlation with the processing methods used. The GAN model, in our opinion, offers the following advantages:

- The GAN framework can be used to model any type of material system.
- The generator once trained can generate an arbitrarily large number of unique microstructures.
- Although the GAN model needs a substantial amount of computing power to train, it is quite efficient when it comes to generating synthetic microstructures.

Despite being trained on an extremely small dataset (598 images), our GAN model offers decent fidelity. We believe that the variation and quality of the images can be improved by using a large dataset. Also, the trained model can be used in transfer learning for other steel microstructure datasets.

This GAN framework can be included into a larger framework to establish Process-Structure-Property (PSP) linkages. The generated microstructures can be added to an already available dataset to improve performance for classification of microconstituents [18].

155 6. Acknowledgement

7. Data availability

The data used in this work was publicly made available by DeCost et al. [8] [here](#). The pre-trained model and code used in this work can be found [here](#).

References

- 160 [1] G. B. Olson, Computational design of hierarchically structured materials, *Science* 277 (5330) (1997) 1237–1242. [arXiv:https://science.sciencemag.org/content/277/5330/1237.full.pdf](#), doi:10.1126/science.277.5330.1237.
URL <https://science.sciencemag.org/content/277/5330/1237>
- 165 [2] D. T. Fullwood, S. R. Niezgodka, B. L. Adams, S. R. Kalidindi, Microstructure sensitive design for performance optimization, *Progress in Materials Science* 55 (6) (2010) 477–562. doi:<https://doi.org/10.1016/j.pmatsci.2009.08.002>.
URL <https://www.sciencedirect.com/science/article/pii/S0079642509000760>
- 170 [3] A. Cecen, H. Dai, Y. C. Yabansu, S. R. Kalidindi, L. Song, Material structure-property linkages using three-dimensional convolutional neural networks, *Acta Materialia* 146 (2018) 76–84. doi:10.1016/j.actamat.2017.11.053.
- 175 [4] R. Cang, H. Li, H. Yao, Y. Jiao, Y. Ren, Improving direct physical properties prediction of heterogeneous materials from imaging data via convolutional neural network and a morphology-aware generative model, *Computational Materials Science* 150 (2018) 212–221. doi:<https://doi.org/10.1016/j.commatsci.2018.03.074>.
180 URL <https://www.sciencedirect.com/science/article/pii/S0927025618302337>

- [5] Z. Yang, X. Li, L. Catherine Brinson, A. N. Choudhary, W. Chen, A. Agrawal, Microstructural materials design via deep adversarial learning methodology, *Journal of Mechanical Design* 140 (11). doi:10.1115/1.4041371.
185 URL <http://dx.doi.org/10.1115/1.4041371>
- [6] D. P. Kingma, M. Welling, An introduction to variational autoencoders, *CoRR* abs/1906.02691. arXiv:1906.02691.
URL <http://arxiv.org/abs/1906.02691>
- 190 [7] I. J. Goodfellow, J. Pouget-Abadie, M. Mirza, B. Xu, D. Warde-Farley, S. Ozair, A. Courville, Y. Bengio, Generative adversarial networks, *NIPS'14: Proceedings of the 27th International Conference on Neural Information Processing Systems - Volume 2* arXiv:1406.2661.
- [8] B. DeCost, M. Hecht, T. Francis, B. Webler, Y. Picard, E. Holm, Uhcsdb: 195 Ultrahigh carbon steel micrograph database: Tools for exploring large heterogeneous microstructure datasets, *Integrating Materials and Manufacturing Innovation* 6. doi:10.1007/s40192-017-0097-0.
- [9] B. DeCost, T. Francis, E. Holm, Exploring the microstructure manifold: Image texture representations applied to ultrahigh carbon steel microstructures, *Acta Materialia* 133. doi:10.1016/j.actamat.2017.05.014.
200
- [10] S. Zhao, Z. Liu, J. Lin, J. Zhu, S. Han, Differentiable augmentation for data-efficient GAN training, *CoRR* abs/2006.10738. arXiv:2006.10738.
URL <https://arxiv.org/abs/2006.10738>
- [11] M. Mirza, S. Osindero, Conditional generative adversarial nets, *CoRR* 205 abs/1411.1784. arXiv:1411.1784.
URL <http://arxiv.org/abs/1411.1784>
- [12] A. Brock, J. Donahue, K. Simonyan, Large scale GAN training for high fidelity natural image synthesis, *CoRR* abs/1809.11096. arXiv:1809.11096.
URL <http://arxiv.org/abs/1809.11096>

- 210 [13] P. Zhou, L. Xie, B. Ni, Q. Tian, Omni-gan: On the secrets of cgans and beyond, CoRR abs/2011.13074. [arXiv:2011.13074](https://arxiv.org/abs/2011.13074).
URL <https://arxiv.org/abs/2011.13074>
- [14] D. Kingma, J. Ba, Adam: A method for stochastic optimization, International Conference on Learning Representations.
215 URL <https://arxiv.org/abs/1412.6980>
- [15] A. Paszke, S. Gross, F. Massa, A. Lerer, J. Bradbury, G. Chanan, T. Killeen, Z. Lin, N. Gimelshein, L. Antiga, A. Desmaison, A. Kopf, E. Yang, Z. DeVito, M. Raison, A. Tejani, S. Chilamkurthy, B. Steiner, L. Fang, J. Bai, S. Chintala, Pytorch: An imperative style, high-
220 performance deep learning library (2019) 8024–8035.
URL <http://papers.neurips.cc/paper/9015-pytorch-an-imperative-style-high-performance-deep-learning-library.pdf>
- [16] T. Salimans, I. J. Goodfellow, W. Zaremba, V. Cheung, A. Radford, X. Chen, Improved techniques for training gans, CoRR abs/1606.03498.
225 [arXiv:1606.03498](https://arxiv.org/abs/1606.03498).
URL <http://arxiv.org/abs/1606.03498>
- [17] M. D. Hecht, Effects of Heat Treatments and Compositional Modification on Carbide Network and Matrix Microstructure in Ultrahigh Carbon Steels
230 [doi:10.1184/R1/6716156.v1](https://doi.org/10.1184/R1/6716156.v1).
URL https://kilthub.cmu.edu/articles/thesis/Effects_of_Heat_Treatments_and_Compositional_Modification_on_Carbide_Network_and_Matrix_Microstructure_in_Ultrahigh_Carbon_Steels/6716156
- [18] S. M. Azimi, D. Britz, M. Engstler, M. Fritz, F. Mücklich, Advanced Steel
235 Microstructural Classification by Deep Learning Methods
[doi:10.1038/s41598-018-20037-5](https://doi.org/10.1038/s41598-018-20037-5).
URL <https://doi.org/10.1038/s41598-018-20037-5>

Appendix A. Architectural details

In this work, we aim to establish a processing-structure relationship via
240 multi-conditional image generation. BigGAN is more intuitive for multi-conditional
scenario since it provides class conditional information at multiple levels of the
generator as opposed to just providing it at the initial level which is the case
for typical GAN architectures. This is illustrated in figure A.7.

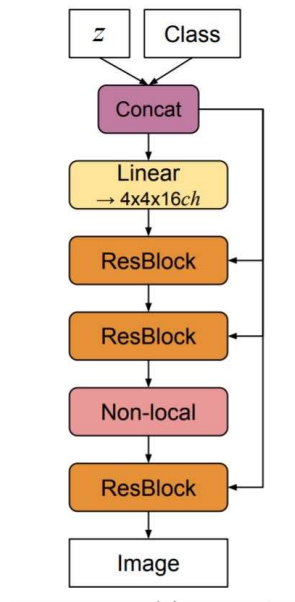


Figure A.7: Layout of the architecture for BigGAN-deep generator [12]

As mentioned earlier, we modify the BigGAN-deep to be better suited for the
245 task at hand. We use three embeddings for annealing temperature, annealing
time and cooling method as opposed to just one. We are not using a projection
style generator . We observed that the model collapsed fairly quickly with a de-
fault latent dimension of 128. Therefore, we increase the latent space dimension
to 384 to avoid collapse as increasing the latent space dimension gives the model
250 more degrees of freedom to fit the individual samples, thereby increasing the
quality of generated images. The aforementioned modifications can be observed
by comparing figure A.8 and A.9.

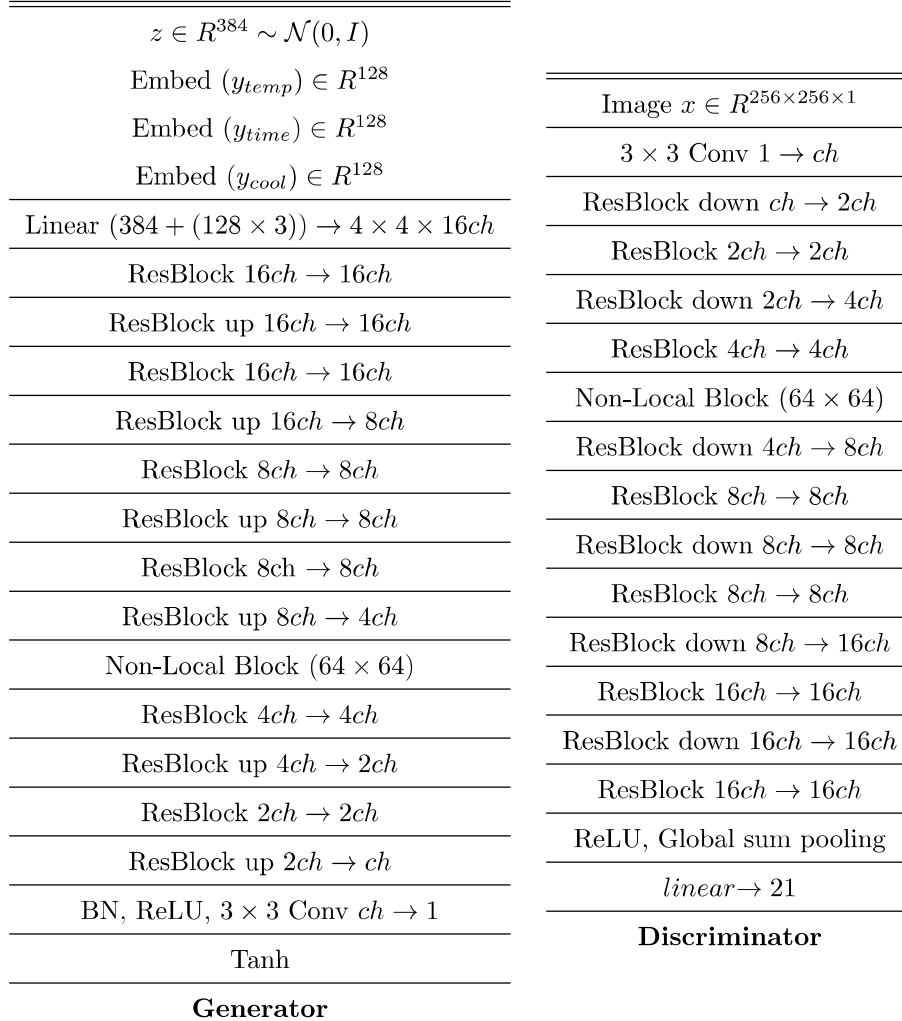


Figure A.8: Our Architecture for 256×256 images. $ch = 64$

$z \in R^{128} \sim \mathcal{N}(0, I)$	Image $x \in R^{256 \times 256 \times 3}$
Embed (y) $\in R^{128}$	3×3 Conv 1 $\rightarrow ch$
Linear $(128 + 128) \rightarrow 4 \times 4 \times 16ch$	ResBlock down $ch \rightarrow 2ch$
ResBlock $16ch \rightarrow 16ch$	ResBlock $2ch \rightarrow 2ch$
ResBlock up $16ch \rightarrow 16ch$	ResBlock down $2ch \rightarrow 4ch$
ResBlock $16ch \rightarrow 16ch$	ResBlock $4ch \rightarrow 4ch$
ResBlock up $16ch \rightarrow 8ch$	Non-Local Block (64×64)
ResBlock $8ch \rightarrow 8ch$	ResBlock down $4ch \rightarrow 8ch$
ResBlock up $8ch \rightarrow 8ch$	ResBlock $8ch \rightarrow 8ch$
ResBlock $8ch \rightarrow 8ch$	ResBlock down $8ch \rightarrow 8ch$
ResBlock up $8ch \rightarrow 4ch$	ResBlock $8ch \rightarrow 8ch$
Non-Local Block (64×64)	ResBlock down $8ch \rightarrow 16ch$
ResBlock $4ch \rightarrow 4ch$	ResBlock $16ch \rightarrow 16ch$
ResBlock up $4ch \rightarrow 2ch$	ResBlock down $16ch \rightarrow 16ch$
ResBlock $2ch \rightarrow 2ch$	ResBlock $16ch \rightarrow 16ch$
ResBlock up $2ch \rightarrow ch$	ReLU, Global sum pooling
BN, ReLU, 3×3 Conv $ch \rightarrow 3$	Embed(y) $\cdot h +$
Tanh	($linear \rightarrow 1$)
Generator	Discriminator

Figure A.9: Original BigGAN-deep architecture for 256×256 images. $ch = 64$